Available online at www.sciencedirect.com
SCIENCE DIRECT®
PERGAMON
International Journal of Multiphase Flow 29 (2003) 475–494
International Journal of Multiphase Flow
www.elsevier.com/locate/ijmulflow

Bi-power law correlations for sediment transport in pressure driven channel flows

J. Wang [a], D.D. Joseph [a,*], N.A. Patankar [b], M. Conway [c], R.D. Barree [d]

[a] *Department of Aerospace Engineering and Mechanics, University of Minnesota, 107 Akerman Hall, 110 Union Street SE, Minneapolis, MN 55455, USA*
[b] *Department of Mechanical Engineering, Northwestern University, Evanston, IL 60208, USA*
[c] *STIM-LAB, Duncan, OK 73534, USA*
[d] *Barree and Associates LLC, Lakewood, CO 80235, USA*

Received 27 February 2002; received in revised form 5 November 2002

Abstract

Power law correlations for sediment transport in pressure driven channel flow was derived in the previous work of the authors. Those correlations can be used as predictive tools in the fracturing industry but they are in implicit forms. New data from slot experiments for fractured reservoir were collected which enable us to derive correlations in explicit forms and applicable over a wide range of data. In this paper we present correlations for bed load transport of slurries as a composition of *bi-power laws* in the proppant and fluid Reynolds number with exponents and prefactors expressed as logarithmic functions of dimensionless sedimentation numbers. The bed load transport correlations are very accurate and are apparently the only such in the published literature.

1. Introduction

A good description of the problem of proppant placement in fractured reservoir in which the present work is framed can be found in the recent paper by Patankar et al. (2002). Only small parts of that description need to be repeated here to make this document easy to understand. Hydraulic fracturing is a process often used to increase the productivity of oil and gas wells. A fluid–proppant mixture is injected through a well bore to be stimulated, at sufficient pressure to open a vertical fracture penetrating from the well bore far into the pay zone. Fig. 1 shows the side

* Corresponding author. Tel.: +1-612-625-0309; fax: +1-612-626-1558.
E-mail address: joseph@aem.umn.edu (D.D. Joseph).

0301-9322/03/$ - see front matter © 2003 Elsevier Science Ltd. All rights reserved.
doi:10.1016/S0301-9322(02)00152-0

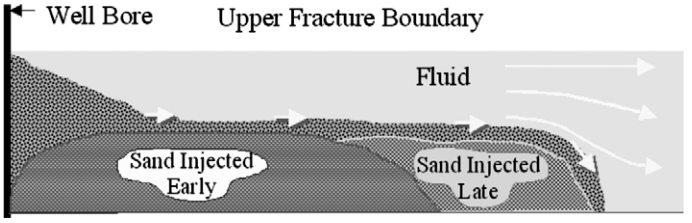

Fig. 1. Sand (proppant) transport in a fractured reservoir (Patankar et al., 2002).

view of the crack. A mound of proppant develops and grows until the gap between the top of the crack and the mound reaches an equilibrium value; this value is associated with a critical condition. For velocities below critical the mound gets higher and spreads laterally; for larger velocities proppant is washed out until the new equilibrium height and velocity are established (Kern et al., 1959).

The major objective of this paper is to process the experimental data on proppant transport in slots from STIM-LAB [1] using the method of correlations. The resultant engineering correlations for erosion and bed load transport can be used to predict proppant placement in the crack.

The method of correlations applied to real or to numerical experiments is a way to *derive formulas and analytic expressions from the processing of data.* Generating correlations from experiments is an old method which many industrial applications are based on but it has come to have a bad name, viewed as empirical and not fundamental. However, used with care and understanding of the physics of the problem, correlation method can generate outstanding results. A good example is the Richardson–Zaki correlation (1954) which is obtained by processing the data of fluidization experiments. Richardson–Zaki correlation describes the complicated dynamics of fluidization by drag and is widely used for modeling the drag force on particles in solid–liquid mixtures.

Our enthusiasm for correlations has to do with the surprising emergence of correlations from the simplest kind of post-processing of our numerical experiments. We have done lift correlations for single particle (Patankar et al., 2001a) and for the bed expansion of many particles in slurries (Patankar et al., 2001b). The procedure we follow is to plot the results of our simulations in log–log plots of the relevant dimensionless variables. The surprise for us is that these plots frequently come up as straight lines giving rise to power laws which is not predictable or at least far from obvious. For example, a single particle will lift-off in a Poiseuille flow at a certain Reynolds number $R = Ud/v$ for a given settling Reynolds number $R_G = \rho_f(\rho_p - \rho_f)gd^3/\eta^2$. When we plotted the lift-off criterion from about 20 points we found that $R = aR_G^n$ with an intercept a and a slope n in the log–log plot. The straight lines are impressively straight and we generated such correlations for lift to equilibrium, for the bed expansion of many particles and in non-Newtonian fluids. The prediction of the power laws for proppant transport from DNS is verified by the engineering correlations obtained from experimental data in Patankar et al. (2002). Patankar et al. processed the data from slot experiments for fractured reservoirs on log–log plots and generated power law

[1] STIM-LAB is a research lab in Duncan, OK, which is supported by a consortium of oil production and oil service companies. STIM-LAB has been collecting data on proppant transport in slots for 15 years.

correlations with a parameter dependent power. The existence of such power laws is an expression of self-similarity, which has not yet been predicted from analysis or physics. The flow of dispersed matter appears to obey those self-similar rules to a large degree (Barenblatt, 1996).

We can get power laws when only two variables are at play; when there are three variables or more, it would appear that we get different power laws separated by transition regions. This is certainly the case for the Richardson–Zaki correlation; it has one power law relating the fluidization velocity to the solids fraction at low Reynolds number, and another at high Reynolds number with a Reynolds number-dependent transition between. The Richardson–Zaki correlation is an example of what Barenblatt (1996) calls "incomplete self-similarity" because of the dependence of the power on the Reynolds number, a third parameter. We got such correlations between three variables for slurries, and from numerical experiments (Choi and Joseph, 2001; Patankar et al. 2001b, 2002; Pan et al., 2002; Joseph and Ocando, 2002; Joseph, 2002).

Here we encounter the yet more complicated situation in which four or five parameters enter and we find a new type of solution in bi-power law correlations. The correlations faithfully describe the erosion and bed load transport in a slot under a wide variety of conditions.

2. Experimental setup

The experimental setup used by STIM-LAB was described thoroughly in Patankar et al. (2002). Here we provide a brief description of the apparatus used by STIM-LAB where the transport of proppant in a horizontally oriented slot could be observed. Fig. 2 shows the apparatus

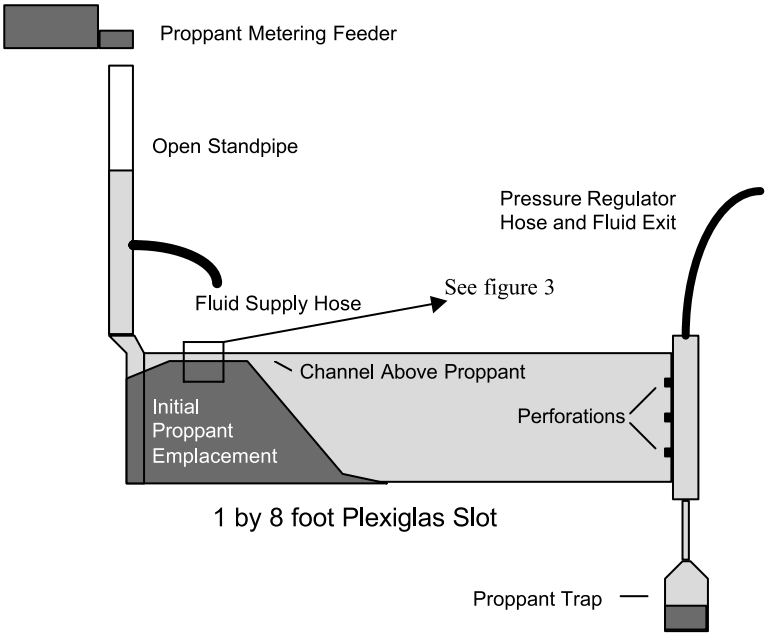

Fig. 2. The experimental setup for proppant transport. Proppant and fluid are added at the left where they enter over the full height of the slot. Materials exit at the right through perforations (Patankar et al., 2002).

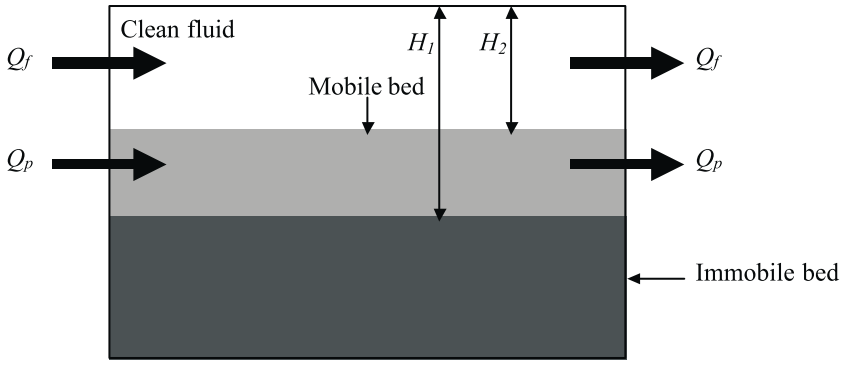

Fig. 3. Proppant transport in thin fluids at steady state conditions. In Case 1 only fluid is pumped, $Q_P = 0$, $H_1 = H_2$; the particles are immobile. In Case 2 proppants are also injected, $Q_P \neq 0$, $H_1 \neq H_2$; there is a mobile bed of height $H_1 - H_2$. The channel width $W = 7.94$ mm (Patankar et al., 2002).

schematically. Proppant and water enter the 8 mm wide slot through an open end that is 30.5 cm tall. The proppant and water then move through the 2.44 m length of the slot where they exit via three 8 mm perforations spaced 7.62 cm apart on the 30.5 cm tall end of the slot. We call attention to that new experiments were conducted in STIM-LAB where more fluids and proppants were used. The correlations presented in this paper describe both old and new data very well.

The proppant bed in the experiments is shown in Fig. 3 and the portion show in Fig. 3 is marked in Fig. 2. There are three distinct zones in the flat bed region. The bottom part of the bed is immobile; it is a stationary porous medium that supports liquid throughput that might be modeled by Darcy's law. Above the immobile bed is a mobile bed in which proppants move by sliding and rolling or advection after suspension or a combination of these modes. Above the mobile bed is the clear fluid zone. At steady state the volumetric fluid flow rate Q_f and the volumetric proppant flow rate Q_p in and out of this region are constant. At steady state, these are equal to the rate at which the fluid and proppant are injected in the slot.

STIM-LAB carried out two types of experiments. In Case 1 only fluid is pumped, $Q_P = 0$, $H_1 = H_2$; the particles are immobile. We call Case 1 *erosion case*. In Case 2 proppants are also injected, $Q_P \neq 0$, $H_1 \neq H_2$; there is a mobile bed of height $H_1 - H_2$. We call Case 2 *bed load transport case*. The channel width $W = 7.94$ mm. A simplified description of the experiment is that a bed of proppant is eroded by the flow of water. When proppant is not injected as in Case 1, the faster the flow of water the deeper is the channel above the proppants. We are seeking to predict the height above the channel for the given fluid flow rate. In Case 2, we seek to predict both the clear fluid height as well as the mobile bed height as functions of Q_f and Q_p. In the experiments the fluid and the proppant flow rates are controlled and the heights H_1 and H_2 are measured.

3. Experimental correlations for sediment transport

3.1. Dimensionless parameters

The dimensionless parameters in this problem are listed below:

Gravity Reynolds number:

$$R_G = \frac{\rho_f[\rho_p - \rho_f]gd^3}{\eta^2}. \tag{1}$$

Gravity Reynolds number for the fluid:

$$\lambda = \frac{\eta/\rho_f}{W^{3/2}\sqrt{g}} \quad \left(\frac{1}{\lambda^2} = \frac{\rho_f^2 g W^3}{\eta^2}\right). \tag{2}$$

Note that W is constant in the experiments, hence, λ can be viewed as the dimensionless form for the kinematic viscosity of the fluid η/ρ_f.

Fluid Reynolds number based on channel width:

$$R_f = \frac{\rho_f \widetilde{V} W}{\eta} = \frac{\rho_f Q_f}{W\eta}, \quad \text{where } \widetilde{V} = \frac{Q_f}{W^2}. \tag{3}$$

Proppant Reynolds number based on channel width:

$$R_p = \frac{\rho_p \overline{V} W}{\eta} = \frac{\rho_p Q_p}{W\eta}, \quad \text{where } \overline{V} = \frac{Q_p}{W^2}. \tag{4}$$

Particle diameter/channel width d/W.
Height of bed/channel width H/W.

We are seeking correlations between the height of the bed H_1/W, H_2/W and the prescribed parameters. The dependence of H_1/W and H_2/W on the three Reynolds numbers R_f, R_p and R_G arises from the fundamental mechanics, as shown in our previous DNS works. In the process of fitting the bed load transport data, we found that the presence of the gravity Reynolds number for the fluid λ in the correlations is necessary for satisfactory fitting. Hence, the correlations are in the form $H_i/W = f(R_f, R_p, R_G, \lambda)$ where $i = 1, 2$. H_i ($i = 1, 2$) depend on eight dimensional variables namely ρ_f, ρ_p, d, η, W, Q_p, Q_f and g. The fundamental dimensions are M (mass), L (length), and T (time). The Pi theorem indicates that the total number of dimensionless parameters involved in developing correlations for H_i is six. The number of dimensionless parameters in $H_i/W = f(R_f, R_p, R_G, \lambda)$ is five; one less than the number indicated by the Pi theorem. The reason is that d and W are constant in the experiments, hence, d/W does not appear in the correlations.

3.2. Power law correlations for the erosion case

The erosion case: $H_1 = H_2 = H$ finds the critical condition of the initial motion of the proppant. Only fluid is injected in the channel and the particle bed is immobile. There is an equilibrium value of H corresponding to a given fluid flow rate. When the fluid flow rate is increased beyond the critical value for a given initial height H, the proppants are eroded from the bed and washed out until a new equilibrium height H of the clear fluid region above an immobile bed is achieved for the new flow rate.

Table 1
The prefactor $a(R_G)$ and exponent $m(R_G)$ in the power law correlations for the erosion case

	R_G		
	86.8	521–2.03×10^4	1.00×10^5
a	0.0294	9.36×10^{-4}	5.52×10^{-4}
m	0.618	0.914	0.878

In the erosion case, three dimensionless parameters R_f, H/W, and R_G enter the power law correlation: [2]

$$H/W = a(R_G)R_f^{m(R_G)}. \tag{5}$$

The values of a and m are listed in Table 1 as functions of R_G. Details of the derivation of the power law correlations for the erosion case can be found in Patankar et al. (2002).

3.3. Bi-power law correlations for the bed load transport case

Bed load transport is another name for the transport of sediments. In bed load transport, both fluids and proppants play important roles in determining H_1 and H_2. Therefore we seek correlations for H_1/W and H_2/W in terms of R_f and R_p with the coefficients as functions of R_G and λ. To create correlations, we need data and a data structure. An example of the way the data is structured for processing correlations is given for 20/40 Ottawa in water in Table 2 (ρ_f: 10^3 kg/m^3, ρ_p: 2.65×10^3 kg/m^3, d: 6×10^{-4} m, η: 10^{-3} Pa s, W: 7.94×10^{-3} m, R_G: 3.50×10^3, λ: 4.51×10^{-4}).

We look for correlations in the bi-power law form with five dimensionless parameters involved:

$$\frac{H_1}{W} = c_1(R_G)R_f^{m_1(R_G,\lambda)}R_p^{n_1(R_G)}; \tag{6}$$

$$\frac{H_2}{W} = c_2(R_G)R_f^{m_2(R_G,\lambda)}R_p^{n_2(R_G)}. \tag{7}$$

Following are the procedures we used to achieve the bi-power correlations: (1) Different kinds of proppant and fluid are used in bed load transport experiments and lead to different values of R_G and λ. For each single case, we develop bi-power law correlations of H_1 and H_2. (2) The prefactors and exponents in these correlations are functions of R_G and λ. We implement curve-fitting to find analytical expression for these coefficients. (3) Curve fitting implies that c_1, n_1, c_2 and n_2 can be reasonably approximated by logarithmic functions of R_G. While the trend of m_1, m_2 is less obvious. (4) We use the predicted c_1, n_1, c_2, and n_2 by the logarithmic functions of R_G and vary m_1, m_2 in the bi-power law correlations to match the measured H_1 and H_2 consistently. The new m_1 and m_2 turn out to be also logarithmic functions of R_G, but with slopes and intercepts as functions of λ. (5) With the explicit and analytical expressions for all the coefficients in the bi-power law known:

[2] Shields's (1936) curve also gives the critical condition for the initiation of sediment motion. The Shields parameter S is defined as: $S = \tau/([\rho_p - \rho_f]gd)$, where τ is a measure of the shear stress on the particle bed. If we take $\tau = \eta\widetilde{V}/W$, then $S = ((\eta\widetilde{V})/([\rho_p - \rho_f]gd^2)) = ((R_f[d/w])/(R_G))$. From the Shields's (1936) curve one obtains $S = f_s(\sqrt{R_f}[d/W])$. Eq. (5), applicable for proppant transport in narrow channels has W/H as another parameter. Nothing close to the bi-power law correlations has been put forward for sediment transport.

Table 2
Experimental data for the bed load transport case with 20/40 Ottawa and water

Q_p (m^3/s)	Q_f (m^3/s)	R_f	R_p	H_1 (10^{-2} m)	H_2 (10^{-2} m)	H_1/W	H_2/W
4×10^{-5}	2.44×10^{-4}	3.08×10^{4}	1.34×10^{4}	2.3	0.8	2.90	1.01
4.57×10^{-5}	2.43×10^{-4}	3.06×10^{4}	1.53×10^{4}	2.6	0.7	3.28	0.88
2.86×10^{-5}	2.50×10^{-4}	3.15×10^{4}	9.55×10^{3}	2.3	1	2.90	1.26
1.14×10^{-5}	2.50×10^{-4}	3.15×10^{4}	3.81×10^{3}	2.4	1.5	3.02	1.89
1.14×10^{-5}	3.14×10^{-4}	3.95×10^{4}	3.81×10^{3}	3	2.1	3.78	2.65
3.43×10^{-5}	3.05×10^{-4}	3.84×10^{4}	1.15×10^{4}	2.9	1.5	3.65	1.89
1.14×10^{-5}	3.15×10^{-4}	3.97×10^{4}	3.81×10^{3}	3.1	2.3	3.91	2.90
4.57×10^{-5}	3.03×10^{-4}	3.82×10^{4}	1.53×10^{4}	3	1.4	3.78	1.76
4×10^{-5}	3.05×10^{-4}	3.85×10^{4}	1.34×10^{4}	3	1.5	3.78	1.89
2.86×10^{-5}	3.06×10^{-4}	3.86×10^{4}	9.55×10^{3}	2.9	1.6	3.65	2.02
2.28×10^{-5}	3.06×10^{-4}	3.86×10^{4}	7.61×10^{3}	2.8	1.7	3.53	2.14
1.71×10^{-5}	3.15×10^{-4}	3.97×10^{4}	5.71×10^{3}	3.1	2	3.91	2.52
5.7×10^{-6}	3.14×10^{-4}	3.96×10^{4}	1.90×10^{3}	3.5	2.9	4.41	3.65
2.9×10^{-6}	3.14×10^{-4}	3.95×10^{4}	9.68×10^{2}	4.1	3.6	5.17	4.54
1.4×10^{-6}	3.13×10^{-4}	3.94×10^{4}	4.67×10^{2}	5.1	5	6.43	6.30
4×10^{-7}	3.12×10^{-4}	3.93×10^{4}	1.34×10^{2}	5.8	5.7	7.31	7.18

$c_1(R_G)$, $c_2(R_G)$, $n_1(R_G)$, $n_2(R_G)$, $m_1(R_G, \lambda)$, $m_2(R_G, \lambda)$, we predict H_1 and H_2 and compare them with the experimentally measured values. The analytical expressions $c_1(R_G)$, $c_2(R_G)$, $n_1(R_G)$, $n_2(R_G)$, $m_1(R_G, \lambda)$ and $m_2(R_G, \lambda)$ can be adjusted to obtain the best fit for H_1 and H_2. Hence, we obtain the final form for the analytical expressions: (8)–(13). Then they are inserted to (6) and (7), giving rise to (14) and (15) as the final form for the bi-power law correlations.

Next, we present the analytical expressions for the prefactors and exponents in the bi-power law correlations. These expressions are plotted in Figs. 4–7.

$$c_1 = -2.30 \times 10^{-4} \ln(R_G) + 2.92 \times 10^{-3}; \tag{8}$$

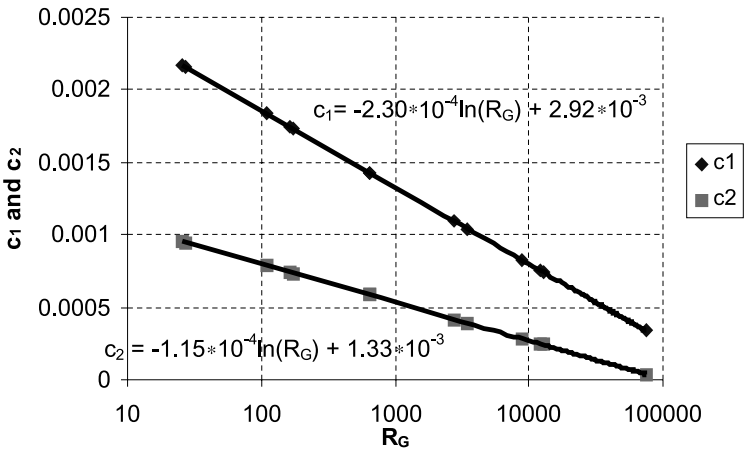

Fig. 4. Prefactors c_1 and c_2 as logarithmic functions of R_G.

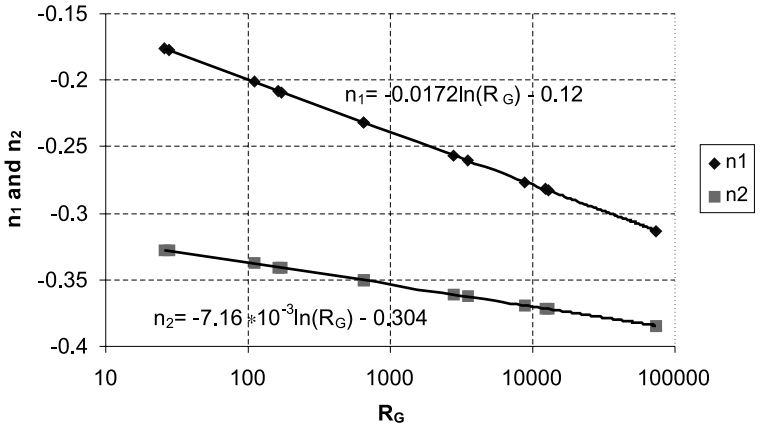

Fig. 5. Exponents n_1 and n_2 as logarithmic functions of R_G.

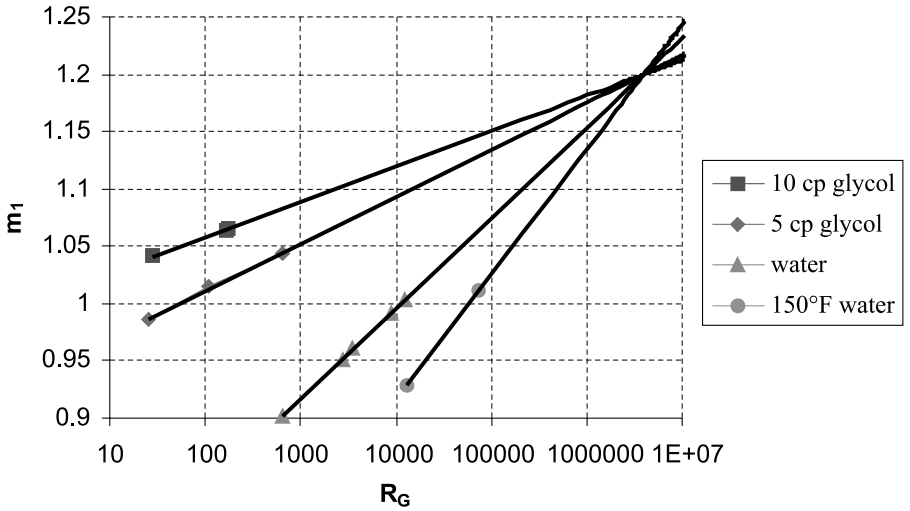

Fig. 6. Exponent m_1 as a logarithmic function of R_G with the slopes and intercepts as functions of λ.

$$c_2 = -1.15 \times 10^{-4} \ln(R_G) + 1.33 \times 10^{-3}; \tag{9}$$

$$n_1 = -0.0172 \ln(R_G) - 0.120; \tag{10}$$

$$n_2 = -7.16 \times 10^{-3} \ln(R_G) - 0.304; \tag{11}$$

$$m_1 = 1.2 - 1.26 \times 10^{-3} \lambda^{-0.428} [15.2 - \ln(R_G)]; \tag{12}$$

$$m_2 = 1.20 - 1.30 \times 10^{-6} \lambda^{-1.28} [11.67 - \ln(R_G)]. \tag{13}$$

From Figs. 4–7, we can see that c_1, n_1, c_2 and n_2 can be represented by logarithmic functions of R_G, while m_1 and m_2 are logarithmic functions of R_G with slopes and intercepts as functions of λ. Eq. (12) implies that for any λ, the logarithmic curve $m_1(R_G, \lambda = \text{constant})$ passes through the

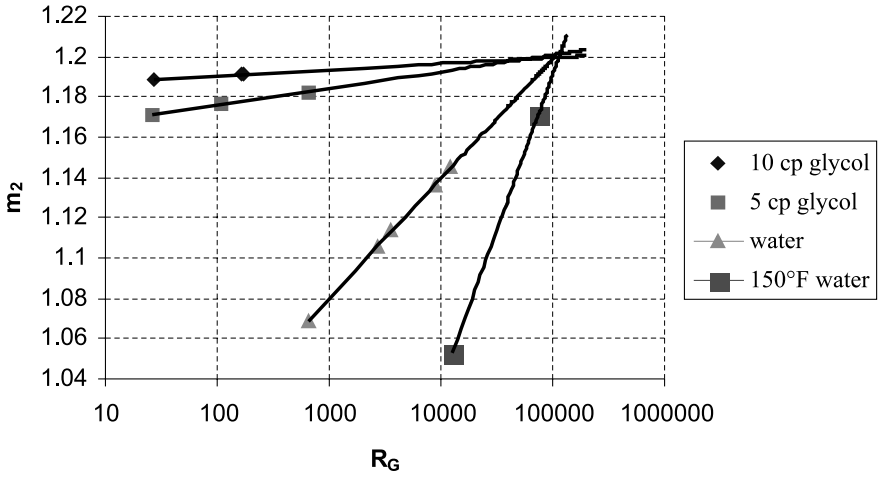

Fig. 7. Exponent m_2 as a logarithmic function of R_G with the slopes and intercepts as functions of λ.

point $(m_1 = 1.2, \ln(R_G) = 15.2)$. Eq. (13) shows that such a point for $m_2(R_G, \lambda)$ is $(m_2 = 1.20, \ln(R_G) = 11.67)$. In Figs. 6 and 7, we can see the two points.

To obtain satisfactory fitting for the data of bed load transport, we find that c_1, n_1, c_2 and n_2 depend on R_G, whereas m_1 and m_2 depend on both R_G and λ. Following is a possible physical explanation for such dependence. m_1 and m_2 are exponents for the fluid Reynolds number and could be sensitive to the kinematic viscosity of the fluid, η/ρ_f. Note that λ is a dimensionless form of the kinematic viscosity of the fluid. In contrast, the prefactors c_1 and c_2 and the exponents of the proppant Reynolds number n_1 and n_2 are less sensitive to the fluid properties. Hence, λ dose not appear in the expressions for c_1, n_1, c_2 and n_2.

In Table 3, the bed load transport experiments with the corresponding R_G and λ are listed. Note that the proppant and fluid used in these experiments and their properties can be found in

Table 3
R_G and λ for bed load transport experiments and the corresponding c_1, c_2, m_1, m_2, n_1 and n_2 predicted by (8)–(13)

R_G	λ	c_1	c_2	n_1	n_2	m_1	m_2
27.5	3.96×10^{-3}	2.16×10^{-3}	9.99×10^{-4}	−0.177	−0.331	1.041	1.189
162	3.96×10^{-3}	1.75×10^{-3}	7.81×10^{-4}	−0.207	−0.345	1.064	1.193
173	3.96×10^{-3}	1.73×10^{-3}	7.72×10^{-4}	−0.209	−0.346	1.065	1.193
25.8	2.03×10^{-3}	2.17×10^{-3}	1.01×10^{-3}	−0.176	−0.331	0.987	1.169
107	2.03×10^{-3}	1.84×10^{-3}	8.31×10^{-4}	−0.201	−0.342	1.012	1.175
644	2.03×10^{-3}	1.43×10^{-3}	6.09×10^{-4}	−0.231	−0.357	1.044	1.184
648	4.52×10^{-4}	1.43×10^{-3}	6.08×10^{-4}	−0.231	−0.357	0.904	1.057
2.82×10^{3}	4.52×10^{-4}	1.09×10^{-3}	4.26×10^{-4}	−0.257	−0.369	0.954	1.106
3.50×10^{3}	4.52×10^{-4}	1.04×10^{-3}	4.00×10^{-4}	−0.260	−0.370	0.961	1.113
8.90×10^{3}	4.52×10^{-4}	8.26×10^{-4}	2.84×10^{-4}	−0.277	−0.378	0.993	1.143
1.59×10^{4}	4.52×10^{-4}	6.92×10^{-4}	2.12×10^{-4}	−0.287	−0.383	1.013	1.163
1.28×10^{4}	2.09×10^{-4}	7.43×10^{-4}	2.40×10^{-4}	−0.283	−0.381	0.929	1.070
7.35×10^{4}	2.09×10^{-4}	3.40×10^{-4}	2.31×10^{-5}	−0.313	−0.395	1.012	1.229

Table 10. c_1, c_2, m_1, m_2, n_1 and n_2 listed in Table 3 are predicted by (8)–(13) corresponding to R_G and λ listed in the first and second columns. These c_1, c_2, m_1, m_2, n_1 and n_2 have been plotted in Figs. 4–7, indicated by points.

Inserting the analytical expressions (8)–(13) into (6) and (7), we get the final form for the bi-power law correlations:

$$\frac{H_1}{W} = [-2.30 \times 10^{-4} \ln(R_G) + 2.92 \times 10^{-3}] R_f^{1.2-1.26\times10^{-3}\lambda^{-0.428}[15.2-\ln(R_G)]} R_p^{[-0.0172\ln(R_G)-0.120]}, \quad (14)$$

$$\frac{H_2}{W} = [-1.15 \times 10^{-4} \ln(R_G) + 1.33 \times 10^{-3}] R_f^{1.2-1.30\times10^{-6}\lambda^{-1.28}[11.67-\ln(R_G)]} R_p^{[-7.16\times10^{-3}\ln(R_G)-0.304]}. \quad (15)$$

We emphasize that Eqs. (14) and (15) are explicit and predictive correlations for proppant transport. By (14) and (15), H_1 and H_2 can be predicted from the prescribed parameters: ρ_f, ρ_p, d, η, W, Q_p, Q_f.

We predict H_1/W and H_2/W by (14) and (15). In Figs. 8 and 9, we plot the predicted values against the experimentally measured data. Ideally, all the points should be on the straight-line $y = x$. It can be seen that the predicted values are in good agreement with the experimental data.

To test this correlation, experiments were conducted in the slot which is 4.88 m long and 1.22 m high. (Note that the correlations are extracted from experiments conducted in the slot which is 2.44 m long and 30.5 cm high.) Following are the prescribed parameters for the experiments in the 4.88 m long slot: 20/40 Ottawa with water, ρ_f: 0.997×10^3 kg/m^3, ρ_p: 2.645×10^3 kg/m^3, d: 5.48×10^{-4} m, η: 9.98×10^{-4} Pa s, W: 7.94×10^{-3} m, R_G: 2.66×10^3, λ: 4.52×10^{-4}.

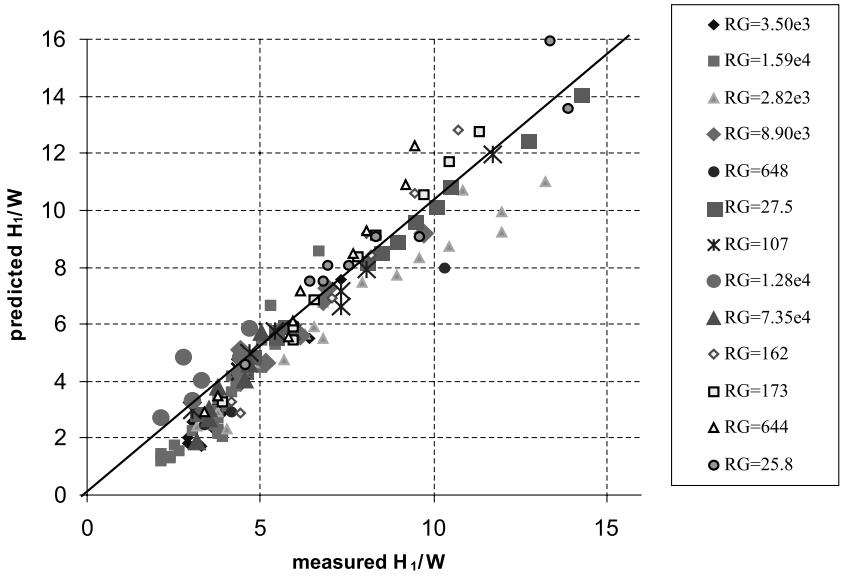

Fig. 8. The predicted values of H_1/W by Eq. (14) versus the experimentally measured values for the cases listed in Table 3.

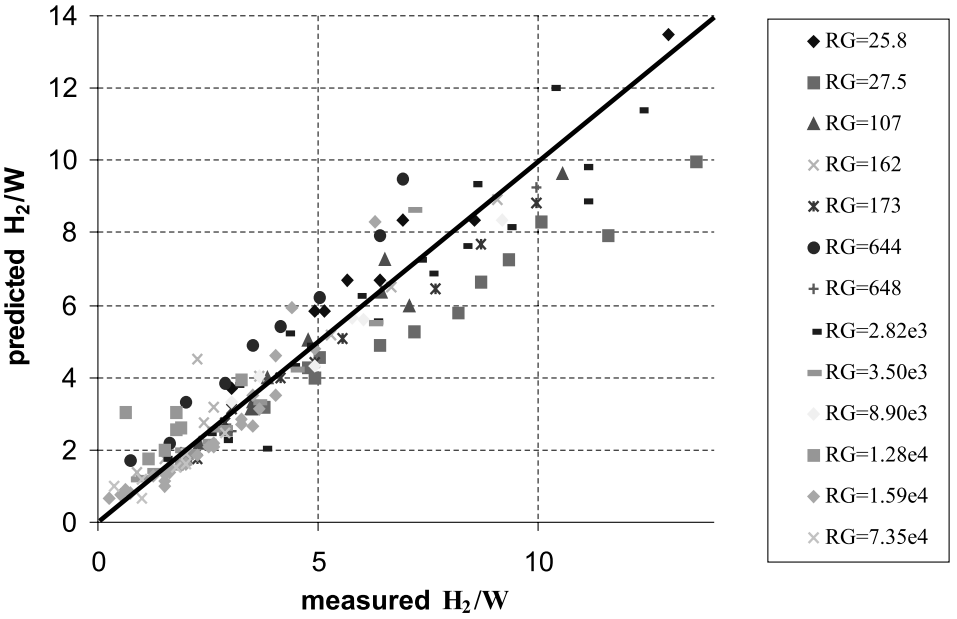

Fig. 9. The predicted values of H_2/W by Eq. (15) versus the experimentally measured values for the cases listed in Table 3.

We can see that the agreement between predicted values of H_1 and H_2 and measured values is encouraging. It is also noted that Table 4 does not show good agreement between predicted and measured values of $H_1 - H_2$. Such inconsistency can be generated in two ways. First, the measurement of the mobile bed height $H_1 - H_2$ is not quite accurate. The total height is fairly reliable measurement but the traction carpet thickness is subject to interpretation especially at higher rates where a clear demarcation between the clear layer and the traction carpet is more difficult to see since some proppant is still transported by viscous forces. The measurements were made by different observers and variations in the recorded heights could be in the order of one centimeter. That is in the same order of $H_1 - H_2$. Due to such errors, the predicted values of $H_1 - H_2$ are not in good agreement of the measured values. Second, our correlations are derived for the total heights and the coefficients in the correlations are adjusted to obtain the best fit for H_1 and H_2. Therefore, the agreement between predicted and measured values of $H_1 - H_2$ is not as good the agreement for H_1 and H_2. The first reason has to do with the experimental uncertainty; the second with the method of processing.

Table 4
The predicted H_1 and H_2 in comparison with the measured H_1 and H_2 in experiments conducted in the slot which is 4.88 m long and 1.22 m high

R_f	R_p	Predicted H_1/W	Predicted H_2/W	Predicted H_1 (m)	Predicted H_2 (m)	Measured H_1 (m)	Measured H_2 (m)
5.14×10^5	1.43×10^4	28.81	25.80	0.229	0.205	0.245	0.243
5.70×10^5	3.82×10^4	24.73	20.14	0.196	0.160	0.202	0.192

The corrlations for H_1/W and H_2/W are bi-power laws in R_f and R_p with the coefficients as logarithmic functions of R_G and λ. In the final form of the correlation, Eq. (14) or (15), eight fitting parameters are used. These parameters emerge as the intercepts and slopes of the logarithmic function and are not arbitrary. Considering the wide range of experimental data covered by the correlations, we believe that the number of fitting parameters is reasonable.

Our bi-power law correlations reveal the hidden self-similarity in the flow of dispersed matter. They are also in a convenient form and applicable to a wide range of data. We believe that our correlations provide a promising way to predict transport of proppant.

3.4. Logistic dose curve fitting for H_1/W and H_2/W

The bi-power law correlation gives good prediction of H_1/W and H_2/W for the bed load transport case. However, it is not compatible with the erosion case. When R_p approaches zero, H_1/W and H_2/W tend to infinity. Therefore we need a different correlation to account for the transition region from the erosion case to the bed load transport case.

We fit the data for H_1/W and H_2/W to a logistic dose curve (see appendix in Patankar et al., 2002 for details) to determine a function valid in the transition region; this fitting effectively combines the power law for the erosion case and the bi-power law for the bed load transport case. We seek to determine the function:

$$\frac{H_1}{W} = C_1 R_f^{M_1} \frac{1}{(1 + (R_p/T_1))^{N_1}} \tag{16}$$

and

$$\frac{H_2}{W} = C_2 R_f^{M_2} \frac{1}{(1 + (R_p/T_2))^{N_2}}. \tag{17}$$

When $R_p = 0$ (the erosion case), (16) and (17) reduce to:

$$\frac{H_1}{W} = C_1 R_f^{M_1}, \tag{18}$$

$$\frac{H_2}{W} = C_2 R_f^{M_2}. \tag{19}$$

For the erosion case, $H = H_1 = H_2$; hence, $C_1 = C_2$, $M_1 = M_2$ and we recover the power law correlation $H/W = a(R_G)R_f^{m(R_G)}$ for the erosion case. When $R_p \gg T_1$ and $R_p \gg T_2$, (16) and (17) reduce to:

$$\frac{H_1}{W} = (C_1 T_1^{N_1}) R_f^{M_1} R_p^{-N_1}, \tag{20}$$

$$\frac{H_2}{W} = (C_2 T_2^{N_2}) R_f^{M_2} R_p^{-N_2}. \tag{21}$$

Therefore, we recover the bi-power law correlations (6) and (7) for the bed load transport case.

Comparing (20) and (21) to (6) and (7), we observe that M_1 and M_2 should be functions of both R_G and λ; hence, the exponent $M_1 = M_2$ in the power law correlations for the erosion case should be functions of R_G and λ. However, most of the erosion experiments were conducted using water

at different temperatures and lead to a small range of λ (see Table 9); we do not have enough data to find an analytical expression $M_1(R_G, \lambda) = M_2(R_G, \lambda)$. However, we find that C_1, M_1, T_1, N_1, C_2, M_2, T_2 and N_2 can be reasonably approximated by functions of a single variable R_G; hence, the coefficients in (16) and (17) are functions of R_G only.

We do not have data for erosion and bed load transport with the same R_G (see Tables 9 and 10) so that we use (16) and (17) to fit data from erosion and bed load transport with different but close R_G:

1. Erosion case with $R_G = 86.8$ and bed load transport case with $R_G = 109$.
2. Erosion case with $R_G = 521$ and bed load transport case with $R_G = 648$.
3. Erosion case with $R_G = 2.29 \times 10^3$ and bed load transport case with $R_G = 2.76 \times 10^3$.
4. Erosion case with $R_G = 1.34 \times 10^4$, 1.45×10^4 and bed load transport case with $R_G = 1.22 \times 10^4$.

The results of fitting erosion with $R_G = 86$ and bed load transport with $R_G = 109$ are presented below:

$$\frac{H_1}{W} = 7.85 \times 10^{-3} R_f^{0.749} \frac{1}{(1 + (R_p/68.23))^{0.112}} \quad (\sigma^2 = 0.951), \tag{22}$$

$$\frac{H_2}{W} = 7.85 \times 10^{-3} R_f^{0.749} \frac{1}{(1 + (R_p/59.24))^{0.156}} \quad (\sigma^2 = 0.946). \tag{23}$$

By (22) and (23), H_1/W and H_2/W are computed and tabulated in Table 5. These computed values are plotted in Fig. 10 in comparison with the experimentally measured values.

Table 5
Data structure for the combination of erosion case with $R_G = 86$ and bed load transport case with $R_G = 109$. H_1/W and H_2/W calculated by Eqs. (22) and (23) are listed in comparison with the experimentally measured values

R_G	R_f	R_p	H_1/W	H_2/W	Computed H_1/W	Error	Computed H_2/W	Error
86.8	897	0	1.76	1.76	1.28	0.24	1.28	0.24
86.8	1.18×10^3	0	2.52	2.52	1.57	0.90	1.57	0.90
86.8	3.63×10^3	0	4.91	4.91	3.63	1.64	3.63	1.64
86.8	1.46×10^4	0	10.71	10.71	10.31	0.16	10.31	0.16
86.8	2.57×10^4	0	15.12	15.12	15.75	0.39	15.75	0.39
109	5.20×10^3	570	2.86	2.30	3.705	0.71	3.29	0.98
109	1.73×10^4	1.90×10^3	8.18	7.06	8.05	0.018	6.79	0.071
109	8.67×10^3	95.1	7.23	6.50	6.32	0.82	6.01	0.25
109	8.67×10^3	143	7.17	6.44	6.15	1.04	5.76	0.46
109	8.67×10^3	285	5.54	4.80	5.80	0.071	5.30	0.25
109	8.67×10^3	571	4.59	3.85	5.43	0.70	4.82	0.96
109	8.67×10^3	951	4.28	3.53	5.16	0.76	4.48	0.91
109	8.67×10^3	1.14×10^3	4.22	3.46	5.06	0.70	4.36	0.81
109	8.67×10^3	1.14×10^3	4.28	3.53	5.06	0.60	4.36	0.70
109	2.60×10^4	1.90×10^3	11.98	10.57	10.90	1.16	9.20	1.87

The error is computed by (calculated value – measured value)^2.

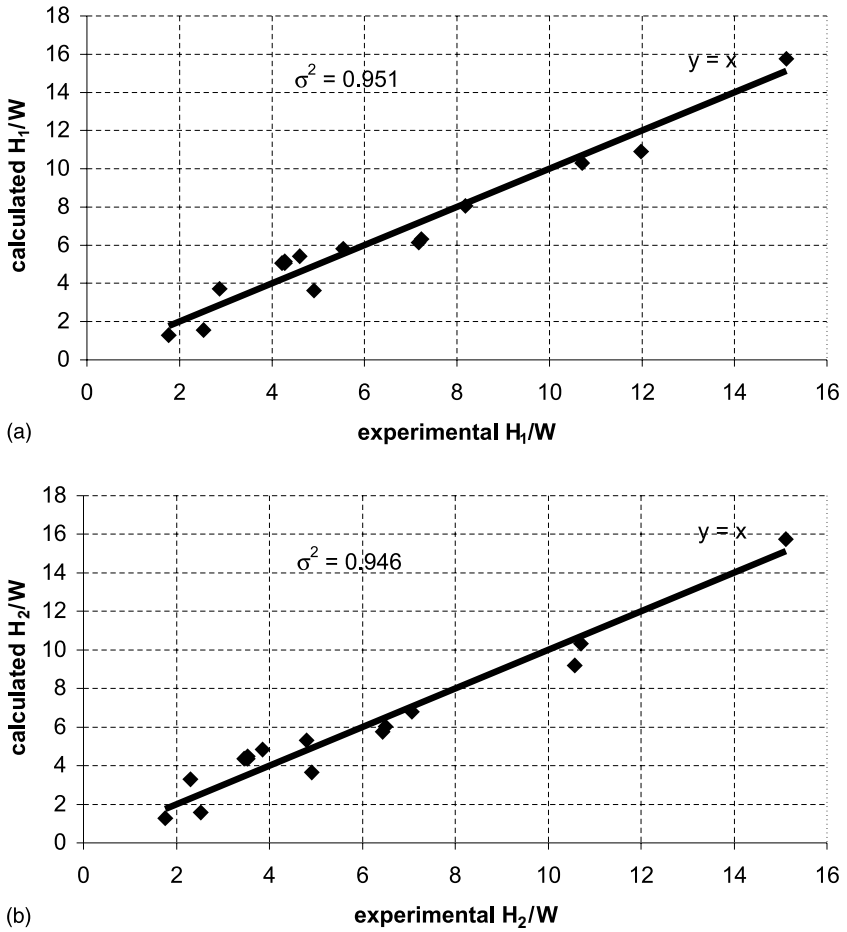

Fig. 10. (a) Experimental H_1/W versus calculated H_1/W using (22). (b) Experimental H_2/W versus calculated H_2/W using (23).

We can see that the computed H_1/W and H_2/W are in good agreement with the experimentally observed values. Cases 2–4 are processed in the same manner and resultant coefficients C_1, M_1, T_1, N_1, C_2, M_2, T_2, N_2 and σ-squared values are listed in Table 6. Note that in Table 6, we use the R_G of the bed load transport case for the combination of data (Figs. 11–13).

Table 6
The coefficients in the logistic dose curve fitting of H_1/W and H_2/W for the data from erosion and bed load transport with close R_G

R_G	C_1	M_1	T_1	N_1	σ^2	C_2	M_2	T_2	N_2	σ^2
109	7.85×10^{-3}	0.749	68.23	0.112	0.951	7.85×10^{-3}	0.749	59.24	0.156	0.946
648	8.56×10^{-4}	0.924	4.173	0.190	0.987	8.56×10^{-4}	0.924	31.60	0.319	0.981
2.76×10^3	1.84×10^{-4}	1.080	3.332	0.234	0.964	1.84×10^{-4}	1.080	9.69	0.300	0.929
1.22×10^4	8.94×10^{-6}	1.361	0.174	0.133	0.945	8.94×10^{-6}	1.361	5.01	0.278	0.945

We only list the R_G of the bed load transport case in the first column.

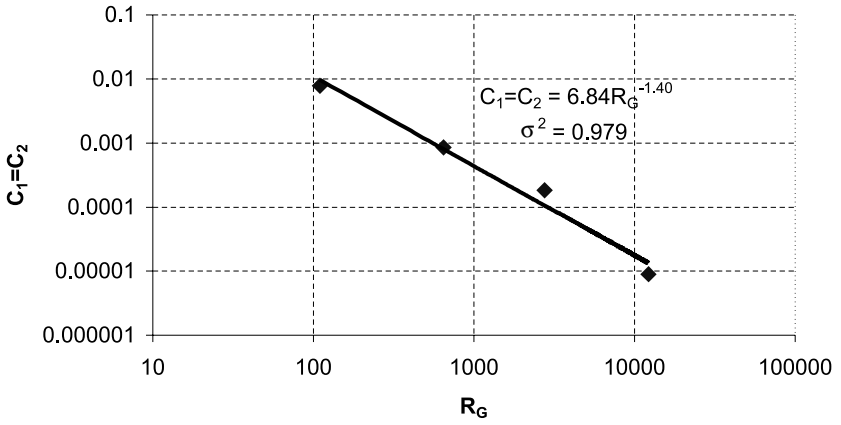

Fig. 11. The coefficient $C_1 = C_2$ as a function of R_G.

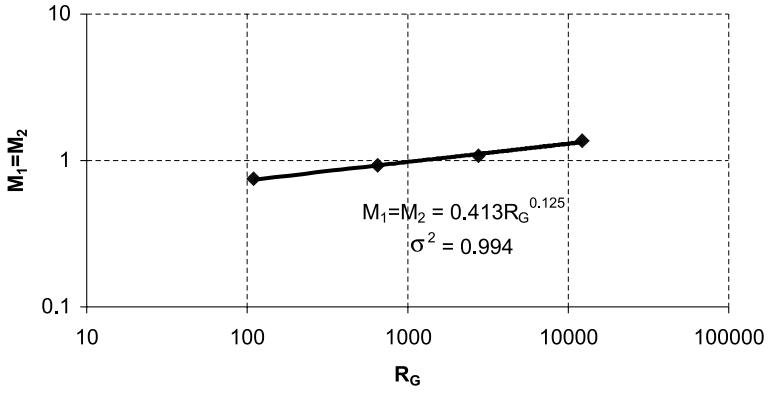

Fig. 12. The coefficient $M_1 = M_2$ as a function of R_G.

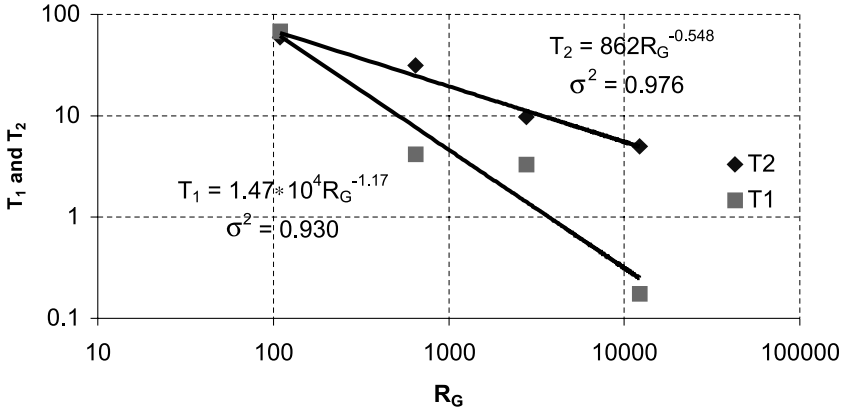

Fig. 13. The coefficient T_1 and T_2 as functions of R_G.

Next we obtain the functions $C_1(R_G)$, $M_1(R_G)$, $T_1(R_G)$, $N_1(R_G)$, $C_2(R_G)$, $M_2(R_G)$, $T_2(R_G)$, and $N_2(R_G)$.

$$C_1 = C_2 = 6.84R_G^{-1.40} \quad (\sigma^2 = 0.979), \tag{24}$$

$$M_1 = M_2 = 0.413R_G^{0.125} \quad (\sigma^2 = 0.994), \tag{25}$$

$$T_1 = 1.47 \times 10^4 R_G^{-1.17} \quad (\sigma^2 = 0.930), \tag{26}$$

$$T_2 = 862R_G^{-0.548} \quad (\sigma^2 = 0.976). \tag{27}$$

We use a natural cubic spline to interpolate $N_1(R_G)$ and $N_2(R_G)$ and the results are plotted in Fig. 15. Because we do not have enough data, the spline interpolation is not reliable and could be significantly changed when more data become available. Such a fitting is at best tentative and is meant to show that expressions for $N_1(R_G)$ and $N_2(R_G)$ could be obtained if we had enough points.

The resultant expressions of the spline interpolation are:

$$N_1 = A_1 + B_1R_G + D_1R_G^2 + E_1R_G^3 \tag{28}$$

where the values of A_1, B_1, D_1, E_1 are listed in the following Table 7:

$$N_2 = A_2 + B_2R_G + D_2R_G^2 + E_2R_G^3, \tag{29}$$

where the values of A_2, B_2, D_2, E_2 are listed in Table 8.

The final correlations:

$$\frac{H_1}{W} = 6.84R_G^{-1.40}R_f^{0.413R_G^{0.125}} \frac{1}{(1 + (R_p/(1.47 \times 10^4 R_G^{-1.17})))^{N_1(R_G)}}, \tag{30}$$

$$\frac{H_2}{W} = 6.84R_G^{-1.40}R_f^{0.413R_G^{0.125}} \frac{1}{(1 + (R_p/(862R_G^{-0.548})))^{N_2(R_G)}}, \tag{31}$$

where $N_1(R_G)$ and $N_2(R_G)$ are expressed in (28) and (29).

Table 7
The coefficients in the spline interpolation for $N_1(R_G)$

	Range		
	109–648	648–2.76×10^3	2.76×10^3–1.22×10^4
A_1	9.43×10^{-2}	7.90×10^{-2}	3.28×10^{-1}
B_1	1.57×10^{-4}	2.28×10^{-4}	-4.26×10^{-5}
D_1	1.46×10^{-8}	-9.47×10^{-8}	3.27×10^{-9}
E_1	-4.45×10^{-11}	1.17×10^{-11}	-8.91×10^{-14}

Table 8
The coefficients in the spline interpolation for $N_2(R_G)$

	Range		
	109–648	648–2.76×10^3	2.76×10^3–1.22×10^4
A_2	1.19×10^{-1}	7.94×10^{-2}	7.62×10^{-1}
B_2	3.33×10^{-4}	5.16×10^{-4}	-2.26×10^{-4}
D_2	3.74×10^{-8}	-2.46×10^{-7}	2.28×10^{-8}
E_2	-1.14×10^{-10}	3.18×10^{-11}	-6.23×10^{-13}

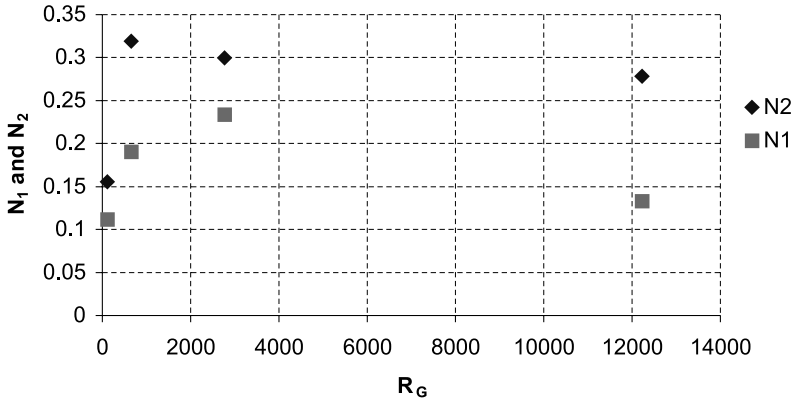

Fig. 14. The coefficients N_1 and N_2 plotted against R_G.

Correlations (30) and (31) can be used to predict H_1/W and H_2/W with the prescribed parameters W, ρ_f, ρ_p, d, η, Q_f and Q_p. These correlations are compatible with both the power law for the erosion case and the bi-power law for the bed load transport case.

We developed the logistic dose curve by fitting the data for erosion and bed load transport using Eqs. (16) and (17). The curve should depend on R_G and λ but we do not have enough data to determine how it depends on λ. This fitting using the dose curve is independent of the previous power law and bi-power law correlations and the resultant Eqs. (30) and (31) do not reduce precisely to Eqs. (5), (14) and (15) at the respective limits. The number of fitting parameters utilized in (30) and (31) is more than in (14) and (15). The reason is that we are not able to find elegant expressions for $N_1(R_G)$ and $N_2(R_G)$ from sparse data (see Fig. 14). We emphasize that the

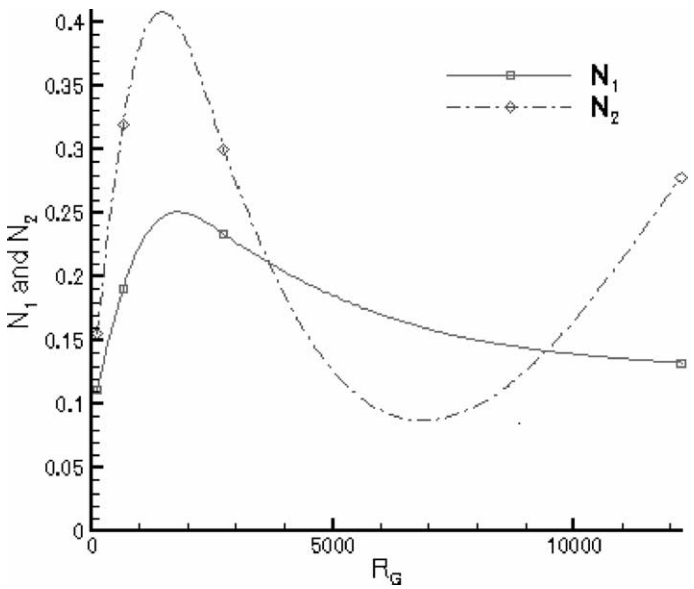

Fig. 15. Use natural cubic spline to interpolate $N_1(R_G)$ and $N_2(R_G)$.

logistic dose curve represents a correlation for transition situations between erosion and bed load transport; it is not as accurate as the power law (5) for erosion or the bi-power law (14) and (15) for bed load transport.

4. Discussion

In a sense our results here realize the opportunity which is presented by digital technology for implementing the old tried and true method of correlations to big data sets. Our mantra is "the secrets are in the data". The same method works well for data from numerical and from real experiments. We have used the following procedure not only for this but also for other multiphase flow processes. First we propose candidates for controlling dimensionless parameters and list the data required to form these numbers in a spreadsheet. Then we identify two parameters and plot the results of the experiments for those two in log–log plots under conditions in which other parameters are fixed. We have a good choice when the plots come up as straight lines in the log–log plot. Here and elsewhere we have had excellent results in this search using the parameters suggested by making the governing sets of PDEs dimensionless. The results of this kind of power law processing is that the slopes and intercepts of the straight lines in log–log plots, or the prefactors and exponents of the power laws these lines imply, depend on the parameters we have fixed. When we look at the variation of these parameters, the prefactors and exponents sometimes are expressible as power laws or logarithmic functions, and sometimes they are not. In any case we may and do implement curve-fitting procedures for the prefactors and exponents to present explicit formulas in analytic form for the prediction of future events. Processing of data when the prefactors and exponents are not expressible by power laws or logarithmic functions, as in the case of logistic dose curve fitting (see Fig. 15), can be carried out by spline or other type of fitting algorithm, but accurate fits are obtained only when there are sufficient data.

We might add that the search for the governing dimensionless numbers in multiphase flow is a way to achieve a deep understanding of the underlying physics. The method of correlations is an excellent procedure to guide the research because the data does not lie.

Acknowledgements

We acknowledge support by the National Science Foundation under grant opportunities for academic liaison with industry (GOALI), by the DOE, Department of Basic Energy Sciences, by a grant from the Schlumberger foundation, from STIM-LAB Inc. and by the Minnesota Supercomputer Institute. NAP acknowledges the support from Northwestern University through startup funds.

Appendix A

Following tables (Tables 9 and 10) give description to the proppant and fluid used in the erosion and bed load transport experiments.

Table 9
Proppant and fluid parameters in erosion experiments

Proppant	Fluid	ρ_f (10^3 kg/m^3)	ρ_p (10^3 kg/m^3)	d (10^{-4} m)	η (10^{-3} Pa s)	W (10^{-3} m)	R_G	λ
60/40 Brady	Water	0.999	2.65	3.42	1.12	7.94	521	5.04×10^{-4}
20/40 Ottawa	Water	0.999	2.65	5.6	1.12	7.94	2.29×10^3	5.04×10^{-4}
20/40 Light Beads	Water	0.999	1.05	6	1.12	7.94	86.8	5.04×10^{-4}
16/30 Banrite	Water	0.999	3.45	8.84	1.12	7.94	1.34×10^4	5.04×10^{-4}
12/20 Badger	Water	0.998	2.65	10.9	1.02	7.94	2.03×10^4	4.59×10^{-4}
16/20 Carbolite	Water	0.998	2.73	9.49	1	7.94	1.45×10^4	4.52×10^{-4}
16/20 Carbolite	180 °F water	0.972	2.73	9.49	0.378	7.94	1.00×10^5	1.76×10^{-4}

Table 10
Proppant and fluid parameters in bed load transport experiments

Proppant	Fluid	ρ_f (10^3 kg/m^3)	ρ_p (10^3 kg/m^3)	d (10^{-4} m)	η (10^{-3} Pa s)	W (10^{-3} m)	R_G	λ
20/40 sand	10 cp glycol	1.11	2.645	5.48	10	7.94	27.5	4.07×10^{-3}
16/30 ceramic	10 cp glycol	1.14	2.73	9.7	10	7.94	162	3.96×10^{-3}
12/20 sand	10 cp glycol	1.14	2.645	10.1	10	7.94	173	3.96×10^{-3}
40/60 sand	5 cp glycol	1.11	2.645	3.38	5	7.94	25.8	2.03×10^{-3}
20/40 sand	5 cp glycol	1.11	2.73	9.7	5	7.94	644	2.03×10^{-3}
20/40 sand	5 cp glycol	1.091	2.65	5.48	5	7.94	109	2.07×10^{-3}
40/60 sand	Water	0.997	2.65	3.38	0.98	7.94	648	4.44×10^{-4}
20/40 sand	Water	0.997	2.65	5.48	0.98	7.94	2.76×10^3	4.44×10^{-4}
20/40 sand	Water	1	2.65	6	1	7.94	3.50×10^3	4.51×10^{-4}
20/40 Bauxite	Water	0.997	3.45	7.09	0.98	7.94	8.90×10^3	4.44×10^{-4}
16/30 ceramic	Water	1	2.71	9	1	7.94	1.22×10^4	4.51×10^{-4}
16/30 ceramic	Water	1	2.73	9.7	0.98	7.94	1.61×10^4	4.42×10^{-4}
20/40 sand	150 °F water	0.981	2.645	5.48	0.455	7.94	1.28×10^4	2.09×10^{-4}
16/30 ceramic	150 °F water	0.981	2.73	9.7	0.455	7.94	7.43×10^4	2.09×10^{-4}

References

Barenblatt, G.I., 1996. Scaling, Self-Similarity and Intermediate Asymptotics. Cambridge University Press.

Choi, H.G., Joseph, D.D., 2001. Fluidization by lift of 300 circular particles in plane Poiseuille flow by direct numerical simulation. J. Fluid Mech. 438, 101–128.

Joseph, D.D., 2002. Interrogations of direct numerical simulation of solid–liquid flow. Available at <http://www.efluids.com/efluids/books/joseph.htm>.

Joseph, D.D., Ocando, D., 2002. Slip velocity and lift. J. Fluid Mech. 454, 263–286.

Kern, T.K., Perkins, T.K., Wyant, R.E., 1959. The mechanics of sand movement in fracturing. Petrol. Trans., AIME 216, 403–405.

Pan, T.-W., Joseph, D.D., Bai, R., Glowinski, R., Sarin, V., 2002. Fluidization of 1204 spheres: simulation and experiment. J. Fluid Mech 451, 169–191.

Patankar, N.A., Huang, P.Y., Ko, T., Joseph, D.D., 2001a. Lift-off of a single particle in Newtonian and viscoelastic fluids by direct numerical simulation. J. Fluid Mech. 438, 67–100.

Patankar, N.A., Ko, T., Choi, H.G., Joseph, D.D., 2001b. A correlation for the lift-off of many particles in plan Poiseuille of Newtonian fluids. J. Fluid Mech. 445, 55–76.

Patankar, N.A., Joseph, D.D., Wang, J., Barree, R.D., Conway, M., Asadi, M., 2002. Power law correlations for sediment transport in pressure driven channel flows. Int. J. Multiphase Flow 28, 1269–1292.

Richardson, J.F., Zaki, W.N., 1954. Sedimentation and fluidization: Part I. Trans. Instn. Chem. Engrs. 32, 35–53.

Shields, A., 1936. Anwendung der aenlichkeitsmechanik und der turbulenzforschung auf die geschiebebewegung. Mitteilungen der Preussischen Versuchsanstalt fur Wasserbau und Schiffbau, Berlin, Germany. Translated to English by Ott, W.P., Uchelen, J.C., California Institute of Technology, CA.